AIP Conference Proceedings

RESEARCH ARTICLE | OCTOBER 03 2022

Medical image learning by integrating image grade and kernel processing into feature extraction

S. Gowriswari ✉; Ramakrishnan Raman; Bhadrappa Haralayya; ... et. al

Check for updates

AIP Conference Proceedings 2519, 030012 (2022)
https://doi.org/10.1063/5.0109761

View Online
Export Citation
CrossMark

Articles You May Be Interested In

Creating a cost-effective network of operational resources for wireless networks

AIP Conference Proceedings (January 2023)

A critical review on the effect of natural fiber in high strength concrete

AIP Conference Proceedings (September 2022)

Diabetic retinopathy detection using an efficient artificial intelligence method

AIP Conference Proceedings (November 2022)

AIP Publishing

Downloaded from http://pubs.aip.org/aip/acp/article-pdf/doi/10.1063/5.0109761/16218230/030012_1_online.pdf

Medical Image Learning By Integrating Image Grade and Kernel Processing Into Feature Extraction

S Gowriswari[1, a)], Ramakrishnan Raman[2, b)], Bhadrappa Haralayya[3, c)] and Nitesh S Vibhute[4, d)]

[1]*Sri Sairam Engineering College, Chennai, Tamil Nadu, India*
[2]*Symbiosis Institute of Business Management, Symbiosis International (Deemed University), Pune, Maharashtra, India*
[3]*Lingaraj Appa Engineering College, Bidar, Karnataka, India*
[4]*Sharnbasva University, Kalaburagi, Karnataka, India*

[a)]Corresponding author: gowrishwari.ice@sairam.edu.in
[b)]raman06@yahoo.com
[c)]bhadrappabhavimani@gmail.com
[d)]niteshsv21@gmail.com

Downloaded from http://pubs.aip.org/aip/acp/article-pdf/doi/10.1063/5.0109761/16218230/030012_1_online.pdf

Abstract. Many strategies of segmentation of medical images are based on supervised voxel classification. These approaches usually work best if a training kit is given that describes the test images by line. However, complications may occur in training and analyzing results, such as due to variations in scanners, procedures, or patient classes, which follow different distributions. Even under the circumstances, weighing pictures based on delivery similarities has demonstrated a substantial improvement in inefficiency. This suggests that part of the training examples represents test information; it makes non-representative data more comparable. Thus, we analyze kernel education to minimize distinctions between training and test data and investigate an additional benefit for picture weighting in kernel learning. Furthermore, we suggest a new image measurement process, minimizing the maximum mean difference between training and test results, improving image weight, and kernel joint optimization. Brain tissue tests, a brain structure lesion, and personalization of the skin suggest that heterogeneous data efficiency significantly boosts both kernel learning and picture weighting when used separately. In this case, MMD weighting works in a manner close to the imaging approaches previously indicated. Integrating picture measurement and matrix modeling will lead to minor performance enhancements, either independently or jointly optimized.
Keywords: Medical Image, Kernel Processing, Feature extraction, Measurement, brain structure.

INTRODUCTION

For biomedical science and clinical practice, the classification of biological images in different organs and structures is important. Automatic separation is necessary since three-dimensional images are manually segmented and very time-consuming, and subject to variations between and between observers. Many automated segmentation processes use a video-supervised classification [1]. A class judgment (which substance or composition) is made per voxel by good communication in a manually noted training sequence

Such techniques were used in brain MRI, for example, for segmentation of whole-brain brain tissue, white matter segmentation, and brain structure segmentation [2]. However, in the event of such inconsistencies between preparation and research material, such as separate scanners, cosmetic tests, or discrepancies between patient classes, the drawback for supervised learning approaches would deteriorate efficiency. People form can respond to these variations quickly [3]. However, supervised learning approaches can deal with image discrepancies, as they also contribute to a discrepancy between training distribution and specified test distribution on the function space.

The First International Conference on Advances in Computational Science and Engineering
AIP Conf. Proc. 2519, 030012-1–030012-7; https://doi.org/10.1063/5.0109761
Published by AIP Publishing. 978-0-7354-4204-7/$30.00

Transfer learning approaches are structured to deal with discrepancies among development and test content, including sample distribution differences. Many transfer learning methods presented so far in the segmentation of the medical picture are based on samples of weightings [4]. The calculation of individual samples or training pictures may be carried out. Image weighting provides the advantage that no labeled training details from the test sensor are required to cope with the discrepancy between detectors relative to sample measurement.

These methods of weighting have historically only been provided with weight training samples as before. No steps are taken to minimize discrepancies in the representation of training and test samples [5]. A procedure for picture weighting should use a training picture only, as is the case, or it can be assigned a weight of zero. We suggest, therefore, merging image measurement with a data augmentation step to get the distribution of data between the training and test data more identical and to distinguish as far as possible the different classes.

To date, little work has explored the clear transition of image classification for the segmentation of medical images. However, diverse approaches have been introduced in image recognition [6]. Many of them attempt a feature vector, which eliminates the variations in transmission between preparation and study. Since vector projections are often inadequate to resolve discrepancies between data sets, transformations of metric learning methods often occur in high-dimensional kernel space.

Conversely, a kernel that reduces propagation disparities can be explicitly learned. For example, Pan et al. [7] suggest an unregulated method to learn a matrix that makes the distribution of training and tests more comparable by minimizing the average difference between development and test specimens. However, the learning kernel is not designed for classification because the process is not being tracked. In Duan et al., a supervised method is developed to learn a kernel that minimizes MMD between samples from training and testing while simultaneously minimizing a classification error on some labeled kernel samples.

Unfortunately, the different processes developed so far and most of the kernel and metric learning methods are over 1 000 [8]. However, in voxel-wise identification, far more observations can be computer-trained with more than 50,000 samples per picture and are possibly seen as an illustration—the outcome of stronger quality.

LITERATURE SURVEY

Object calculation improves significantly in weighting all training examples for all four experiments: brain tissue of a voxel, injury of white matter, and segmentation of the hippocampus. This compelling advantage of image measurement is the same as previous results. Kullback-Leibler (KL) weighting was conducted far better than other weightings, which were also observed for WML segmentation with highly unequaled classes. The KL weighting here is probably higher than the others [9].

Small pre-delivery bution P (x) In brain tissue methods, because parts and hippocampus segmentation are more important, the best methods were different, and the differences between the three methods of weighting were relatively small. The new mean maximum image difference weighting has the advantage that no transitional PDF estimate is required compared to KL and Bhattacharyya distance weighting. This is particularly advantageous as multiple features are included since PDF calculations scale the difficulty with the number of features quadratically [10].

On the other hand, the estimation time scales for the current implementation of MMD image weighting are quadratic as the number of samples used to refine the measurement BD is O (n). Thus the MMD matrix M in the equation may be worthwhile, whereas KL is O and (n). Research the approach for speeding up MMD calculations. For example, We observed that KL and BD image measurement allocated training images identical synaptic weights. Still, different weight vectors by weighting MMD were assigned to different test images of the same scanner.

Both KL and BD measure differences in density in functional space. MMD tests distances between several samples, meaning that samples need to be shifted in functional areas to turn a training distribution into the evaluation distribution. MMD measures samples. This distance between shifted samples is not taken into account by KL and BD [11]. This might lead to KL and BD finding some training images, which probably are given a high weight over all test images, with average tissue class sizes. The sizes of the different dispersion peaks in our case studies, the three different brain tissues, are more likely to influence MMD, on the other hand, and may thus have a greater impact than KL and BD based on subject differences.

MKL, one of the two methods presented, significantly improved the performance of the Gaussian skin cells and WML segment kernel baseline and was similar to the hippocampus segmentation baseline. Image weighting resulted in all three implementations in greater improvement than MKL, but this increase was not significant for the

Downloaded from http://pubs.aip.org/aip/acp/article-pdf/doi/10.1063/5.0109761/16218230/030012_1_online.pdf

segmentation of WML. With the models were selected of the picture measurement and MKL in total, the picture weighting alone, except the hypothalamus differentiation, improved further [12].

With Cortes et al. focused's kernel alignment method and with the additional term MMD, we found no clear performance difference between MKL. Please note that CKA MKL is based only on training data, so it finds kernel space between classes that makes the training datasets more generalizable. Kernel space can be applied to the MMD term that also eliminates discrepancies among development and test distributions. We showed that both MKL methods provide a new kernel space by following different operating system weights, but the performance in classifications using both techniques was similar [13].

For both methods, no guarantees are available for the classification of the test samples as the resultant kernel space and image weights since no labeled test-distribution samples have been available for training. The additional MMD term may give a kernel space, which reduces differences in distribution among data sets compared to CKA MKL. The addition of the MMD concept offers the benefit of allowing kernel and image weight joint optimization with MMD image weighting. This has the advantage of achieving an optimal joint for kernel and image weights and being more efficient. But on the contrary, in the equation of the setting of the export parameter¯a set value iee.g thus äl= 1 should also be necessary for the use of the MMD term. However, it may be added because we found that productivity is suitable for a wide range of principles for è t.

PROPOSED SYSTEM

We conducted trials for three segmentation tasks of the MRI brain: the segmentation of the brain tissues and the hippocampus. Each voxel inside a manually annotated brain mask was labeled for the segmentation of brain tissues as either white matter grey matter or brain fluid. Each voxel within an automated brain mask was labeled as WML or non- WML for WML segmentation. A multi-atlas registration of the hippocampus was used to identify an area of interest around the amygdala. Per voxel in this ROI has been labeled as neuronal or not. Classifications of strength characteristics are carried out using an SVM classifier. We contrasted SVM efficiency with the random wood classification in an additional study [14].

We also used data from separate databases for these three applications that have been acquired with multiple detectors and imaging parameters. Every image was once segmented into one-way data set-out validation were all images from separate data sets consisting of training data than the test image.

61 images from 5 datasets have been used for the brain tissue segmentation, with the accompanying manual segmentation. All data used for studies are summarised. The MRBrainS Challenge and the Internet Brain Segmentation Archive have two datasets of the Rotterdam Scan Research one. The photos of the BT1, BT2, and BT3 datasets were collected by one scanner, BT4 and BT5 by several scanners (but which images are from the same scanner is unknown). The brain mask and tissues are separated manually into all images. BT3 and BT4 images contain the brain mask; BT1, BT2, and BT5 images do not. Images are contained in the head shield. In contrast to the T1 photos of other tales, pictures from BT2, which are Haste-Odd images, have reversed strength. Therefore, before measuring characteristics, voxel values in the BT2 images were reverted [15].

A total of 40 manually secured photographs of 3 data sets were used for WML segmentation. One from the RSS and three from the MICCAI 2008 MS Lesion Challenge The brain reduction technique was used to construct masks of the brain. We viewed WML1 PD pictures in the same way that WML2 and WML3 T2 pictures were to measure attributes because they were physically identical. We used MR pictures from the Harmonized Protocol (HarP) 4 for the hippocampus experiments. This dataset includes 135 photographs weighted with T1 from the manually annotated hippocampi Alzheimer's disease Neuroimaging Initiative (ADNI) dataset. These 135 pictures were analyzed at 34 locations and a total of 46 scanners. These photos are separated into databases of pictures screened.

We used the same scanner for brain removal. To create brain masks, all images have been rigidly recorded with MNI Space Tool. For amplitude non-uniformity, all images were corrected using the N4 process. Then the 4-Brantford percentile was rescaled to the 0-1 interval within the brain mask to normalize the picture intensities. The preceding characteristics were determined for each series and each voxel. For ÚF = 1, 2, 4 mm3 of brain tissue segments were selected, for WML −F = 0.5, 1, 2 mm 3 were selected based on the ÓF tation= 1, 2,2, 5 mm3 were selected, and the segmentation of hippocampus segmeippocampus was identical to the overall small voxel sizes.

Spatial elements have been added for the segmentation of brain tissue. The following measurements were taken for every voxel: first of all, each brain mask was scaled to [−1, 1] in each orientation, and the source Po was set as the core of the skin mask. The perpendicular distance from here and −F is the negative angle (first [0, μ]), between voxel and o; z shows the location of voxel and O and anterior and posterior axes in a cranial-caudal axis. WML has

Downloaded from http://pubs.aip.org/aip/acp/article-pdf/doi/10.1063/5.0109761/16218230/030012_1_online.pdf

no spatial features because lesions will occur between training and test images at various locations. No spatial features have been used for hippocampus segmentation because spatial information has been encoded in the chosen ROI.

RESULTS AND DISCUSSIONS

This resulted in 13 functions for experimenting with brain tissues, 30 features for experimentation with WML, and ten functions for experimentation with the hippocampus. This function was used for the learning of kernels and the weighting of the image. All attributes have been optimized to mean zero unit variation per picture for all implementations. Training on any pictures from multiple datasets did not use a function reduction. For the segmentation of the hippocampus, all voxels in an ROI were separated into the prefrontal cortex or non-hippocampus as shown in Figure 1.

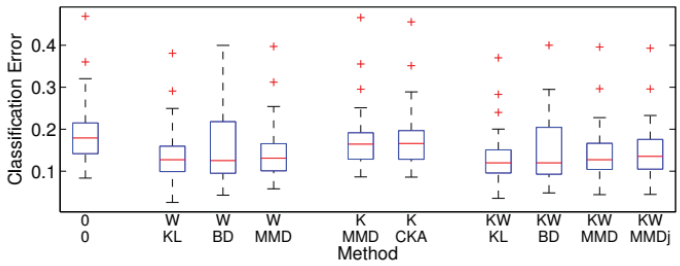

FIGURE 1. Classification performance

Vocals within the brain mask are categorized as white matter, grey matter, CSF, WML, and non-WML, respectively, for brain tissue segmentation and WML segmentation. We analyze the output of 10 approaches, divided into four groups, including Cat. Vocals in the train and test data 0, a baseline approach that does not use image or kernel knowledge; Cat W, three methods of image percentages, KL, MMD, BD, Pet. K, two separate kernel transfer learning, CKA, corresponding to with = 0, and MMD, corresponding to Equationwith functions = 0. CKA, in combination with KL, BD, MMD image weighting, and MMD kernel learning, in combination with image weighing, the kernel and weight optimization are carried out jointly as per Equation 16: K&W, four ways to integrate MCL with image weighting. Figure 2 shows the training image modeling.

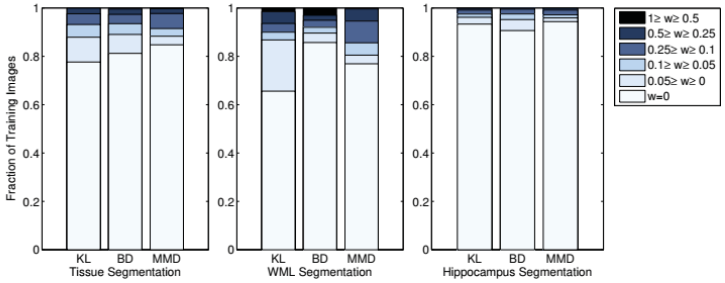

FIGURE 2. Training image modeling

It summarises all comparative approaches. A Gaussian kernel with kernel parameter ŚG, which was calculated by cross-validation, was used while no MKL was used. For MKL, we would use a total of 60 base kernels consisting of 4 different kernel forms, Duan and a Kernel of Gaussian, Laplacian kernel, and the inverse square distance. Both classifier output has been assessed in terms of brain tissue classification errors and WML checks. Output was calculated in the Dice overlap for hippocampus experiments. Pairs in all three implementations have calculated differences between the two methods.

Downloaded from http://pubs.aip.org/aip/acp/article-pdf/doi/10.1063/5.0109761/16218230/030012_1_online.pdf

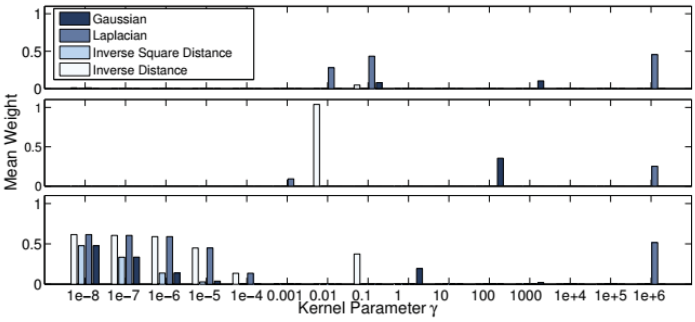

FIGURE 3. System performance

The meaning threshold of a two-tailed t-test at P = 0.05. We used different classifiers on the left and right amygdala for the hippocampus studies, which surpassed a combined classifier. On the left and right hippocampus, the performance on the hippocampus section was averaged. We used implementation in LibSVM for all SVM classification. The inner-reflective Newton method was used to maximize the kernel and the image weight.

Kernel parameters and picture weights smaller than 0.01 were set to null after optimization we have conducted tests on an RF rather than an SVM, as RF is widely used to segmentation the medical picture over SVM. We used 100 trees and other default parameters close to previous work on the weighting of images for medical image segmentation. We have used the implementation of MatlabTreeBagger. We used kernel PCAfor experimentation in Subsections K and K&W because RFs cannot manage kernels directly. In this case, the d key components with the most variation were derived from the kernel and used as development and test datasets functions. The number of features in the initial data is equal to the number. Figure 3 shows the system performance.

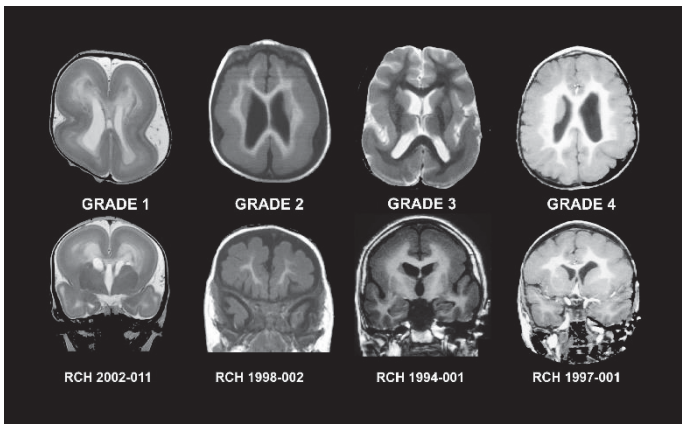

FIGURE 4. Sample test images

Training and research sets consist of a uniform random choice of voxels inside a brain mask to segmentation brain tissue. For WML segmentation, only voxels have been chosen for training and test with a normalized FLAIR strength above 0.75, as WMLs are bright on the FLAIR pictures. To discard non-WML voxels with WML voxels, a value of 0.75 has been selected. As a result, most CSF pixel intensities and some GM voxels have been excluded, with almost every voxel in WM and WML retained. The following was sampled WML, and non-WML voxel in training sets and the test sets overwhelmingly, rendering 20% of the voxel picked by the dataset compose of WML voxels. The sorting took place because the previous likelihood of WML being a voxel is so limited that all voxels will be counted as non-WML feature vectors. In comparison to the description, the processor knowledge and picture weight are calculated on a direct proportion of sampled datasets. Figure 4 shows the sample test images.

Both testing images from multiple detectors were not rigidly recorded for the test picture in the hippocampus classification. The atlas of training images is accordingly transformed, and an ROI compound of all voxels on which at least 10% of atlases vote to be hippocampus was created to pick test samples. Similarly, the training samples were chosen by capturing non-rigidly each other's photos and building an ROI for voxel training. Using the register

Downloaded from http://pubs.aip.org/aip/acp/article-pdf/doi/10.1063/5.0109761/16218230/030012_1_online.pdf

parameters, registration was carried out using the Elastix Registry Toolbox to optimize normalized information. For applications, the MKL and image weighting sets were made up of 1 000 randomly sampled voxels for the training images and the test image for each image.

First, all weight w < 0.01 to zero, followed by a random array of 10 000 voxels for each training image, according to weight vector w, was created for the classifiers' training sets. Both training pictures were measured similarly with the unweighted classifiers. The research collection included all voxels for hippocampus optimization.

CONCLUSION

For example, our approach is readily applicable in practice in multi-center tests because no labeled data from the marketers is needed. The weighting of images may be useful even though those manually noted images are accessible from a test scanner. Although this environment is not checked in this report, we assume the kernel learning combination and picture weighting can be helpful here as well. Throughout this case, the checked test results are furthermore used to guarantee, by optimizing the CKA on test samples instead of training samples, that the kernel is appropriate for the classification of test samples. We compared the added value with Gaussian Scale Functionality only for the Classification technique for image weighting and kernel learning. Even though both image and kernels modeling can, by using different characteristics, classification devices, and different pre-and post-processing, can be extended to other segmentation approaches, image weighting may be implemented in other frameworks, in particular in the form used in this article, in which learning sample was selected depends on the volume of an object.

REFERENCES

1. Cheplygina, A. Van Opbroek, M.A. Ikram, M.W. Vernooij and M. De Bruijne, "Asymmetric similarity-weighted ensembles for image segmentation. In Biomedical Imaging (ISBI)," *13th Interna- tional Symposium on,* pp. 273–277, (2016).
2. Coleman and Y. Li, "An interior trust region approach fornonlin- ear minimization subject to bounds," *SIAM Journal on Optimization,* vol. 6, no. 2, pp. 418–445, (1996).
3. Cortes, M. Mohri and A. Rostamizadeh, "Algorithms for learning kernels based on centered alignment," *Journal of Machine Learning Research,* vol. 13, no. 3, pp. 795–828, (2012).
4. Cortes and V. Vapnik, "Support-vector networks," *Machine Learning,* vol. 20, no. 3, pp. 273–297, (1995).
5. De Boer, H. A. Vrooman, M. A. Ikram, M. W. Vernooij, M. M. B. Breteler, A. Van der Lugt and W.J. Niessen, "Accuracy and repro- ducibility study of automatic MRI brain tissue segmentation methods," *NeuroImage,* vol. 51, no. 3, pp. 1047–1056, (2010).
6. De Boer, H. A. Vrooman, F. Van der Lijn, M. W. Vernooij, M. A. Ikram, A. Van der Lugt, M. Breteler and W.J. Niessen, "White matter lesion extension to automatic brain tissue segmentation on MRI," *NeuroImage,* vol. 45, no. 4, pp. 1151–1161, (2009).
7. Dice, "Measures of the amount of ecologic association between species," *Ecology,* vol. 26, no. 3, pp. 297–302, (1945).
8. Dill, A. R. Franco and M. S. Pinho, "Automated methods for hippocampus segmentation: the evolution and a review of the state of the art," *Neuroinformatics,* vol. 13, no. 2, pp. 1–18, (2015).
9. Duan, I. W. Tsang and D. Xu, "Domain transfer multiple kernel learning," *Pattern Analysis and Machine Intelligence, IEEE Transactions on,* vol. 34, no. 3, pp. 465–479, (2012).
10. Ji, Wei, Shuang Yu, Junde Wu, Kai Ma, Cheng Bian, Qi Bi, Jingjing Li, Hanruo Liu, Li Cheng and Yefeng Zheng, "Learning Calibrated Medical Image Segmentation via Multi-Rater Agreement Modeling," *In Proceedings of the IEEE/CVF Conference on Computer Vision and Pattern Recognition,* pp. 12341-12351, (2021).
11. Orfao, Jarred and Dustin van der Haar, "A Comparison of Computer Vision Methods for the Combined Detection of Glaucoma, Diabetic Retinopathy and Cataracts," *In Annual Conference on Medical Image Understanding and Analysis,* pp. 30-42, (2021). *Springer, Cham.*
12. Gobhinath, S. S. Anandkumar, R. Dhayalan, P. Ezhilbharathi and R. Haridharan, "Human Brain Tumor Detection and Classification by Medical Image Processing," *In 2021 7th International Conference on Advanced Computing and Communication Systems (ICACCS),* vol. 1, pp. 561-564, (2021).

Downloaded from http://pubs.aip.org/aip/acp/article-pdf/doi/10.1063/5.0109761/16218230/030012_1_online.pdf

13. Luo, Xiaoling, Zuhui Pu, Yong Xu, Wai Keung Wong, Jingyong Su, Xiaoyan Dou, Baikang Ye, Jiying Hu and Lisha Mou, "MVDRNet: Multi-View Diabetic Retinopathy Detection by Combining DCNNs and Attention Mechanisms," *Pattern Recognition*, p. 108104, (2021).
14. Reddy, K. Thirupal, M. Madhuri and R. Madana Mohana, "Classification of Medical Image Data Using Advanced Deep Learning And Super Optimization Technique," *Turkish Journal of Physiotherapy and Rehabilitation*, vol. 32, no. 3.
15. B. Ramu, and Navjot Rathour, "A Study of Deep Learning-Based Brain Tumour Segmentation Strategies for MRI Image," *Annals of the Romanian Society for Cell Biology*, vol. 25, no. 6, pp. 15460-15476, (2021).

Downloaded from http://pubs.aip.org/aip/acp/article-pdf/doi/10.1063/5.0109761/16218230/030012_1_online.pdf